RSC Advances

PAPER

View Article Online
View Journal | View Issue

Cite this: *RSC Adv.*, 2024, **14**, 11885

Synergistic effects of the bimetallic Ni–Fe systems and their application in the reductive amination of polyether polyols

Ruiying He, † Zhongpeng Zhu,†* Weiping Zheng, Dandan Jia, Zhaolin Fu, Mingqing Wu, Jie Zhao,* Sheng Wang and Zhiping Tao

Received 5th February 2024
Accepted 6th April 2024

DOI: 10.1039/d4ra00944d

rsc.li/rsc-advances

We report the synthesis of xNi–yFe/γ-Al_2O_3 catalysts which were applied to the reductive amination of polypropylene glycol (PPG) for the preparation of polyether amine (PEA). The catalysts were characterized by N_2-sorption, X-ray diffraction, H_2-temperature programmed reduction, energy-dispersive X-ray spectroscopy, and X-ray photoelectron spectroscopy to reveal the synergistic effect of the bimetallic Ni–Fe-loaded catalysts. It was found that in the reductive amination of PPG to PEA, the conversion and product selectivity of the reaction were closely related to the types of active centers of the catalyst. In particular, the surface Ni^0 content increased by adding Fe as a promoter, with a maximum Ni^0 content on the 15Ni–7.5Fe/Al_2O_3 catalyst, which also led to the highest conversion rate (>99%). In addition, no deactivation was observed after three cycles of reaction carried out by the catalyst.

Introduction

Polyether amines (PEA), as an important functional material, especially in the form of primary amines, have a wide range of industrial applications in the fields of petrochemicals, medical drugs, and daily chemicals.[1] To date, reductive amination is the best way to obtain polyether amines among all main synthesis methods,[2–4] where the reductive amination of polypropylene glycol (PPG) to polyether amine (PEA) over supported metal catalysts involves dehydrogenation, condensation, and hydrogenation steps.[5] Catalysts with dehydrogenation and hydrogenation capabilities are required in the reductive amination process. Currently, transition metals such as Ni, Co, and Pd are mainly used as important active components of the catalysts.[6–8] Considering the cost of catalyst fabrication as well as the operational stability, we prefer to choose nickel-based catalysts for modification.

Various optimization studies involving the addition of promoters to the Ni-based catalysts have been carried out, revealing that alloys formed by bimetallic catalysts can improve catalytic activity. Adriano H. Braga *et al.*[9] loaded a Ni–Co bimetallic catalyst on a $MgAl_2O_4$ carrier for ethanol steam reforming. They discovered that the Ni–Co alloy in the catalyst prevented carbon accumulation on the catalyst surface and improved its stability. Jitendra Kumar Prabhakar *et al.*[10] utilized Ni–Al_2O_3 and Ni–Fe/Al_2O_3 in CO_2 methanation, showing that the catalytic activity of Ni–Fe/Al_2O_3, which contains a Ni–Fe alloy, was significantly superior to that of Ni–Al_2O_3 according to kinetic studies. Xia Xu[11] applied Ni–Fe/Al_2O_3 to the oxidative dehydrogenation of ethane, finding that the catalytic activity of this catalyst was higher at lower reduction temperatures, facilitating ethane dehydrogenation. These examples demonstrate the widespread use of catalysts with alloys in dehydrogenation/hydrogenation reactions, offering both good catalytic effects and economic benefits.

In this work, we investigated the synergistic effect of Ni–Fe bimetallic-loaded catalysts on the reductive amination of PPG (molecular mass = 1000 g mol^{-1}). For this purpose, the synthesized xNi–yFe/γ-Al_2O_3 catalyst was characterized using N_2 adsorption, X-ray diffraction (XRD), H_2-programmed temperature-raising reduction (H_2-TPR), X-ray photoelectron spectroscopy (XPS), and applied in reductive amination reaction.

Experimental

Catalyst preparation

A series of xNi–yFe/Al_2O_3 (x = 15, 10, 2.5; y = 2.5, 5, 7.5, 10, 15) samples were prepared by the incipient wetness impregnation method. These catalysts using a precursor solution of nickel ($Ni(NO_3)_2 \cdot 6H_2O$) and iron ($Fe(NO_3)_3 \cdot 9H_2O$) and a commercial γ-Al_2O_3 support. The impregnated catalysts were dried at 110 °C overnight and then calcined at 500 °C for 3 h under a constant flow of air. In the series of Ni–Fe/γ-Al_2O_3 catalysts, the Ni loading was fixed at 15 wt%, 10 wt% and 2.5 wt% (Ni/Al_2O_3). The final catalysts will thus be referred to as xNi–yFe/Al_2O_3 catalysts, where x denotes the quality ratio of Fe/Ni, and the monometallic Ni loaded on γ-Al_2O_3 will be referred to as Ni/Al_2O_3.

Sinopec Research Institute of Petroleum Processing Co., LTD., Beijing 100083, P. R. China. E-mail: zhuzhongpeng.ripp@sinopec.com

† These authors contributed equally to this work.

Characterization

X-ray photoelectron spectroscopy (XPS) was carried out using a Thermo Fisher ESCALAB Xi+ instrument with a monochromatic Al Kα X-ray source with a spot size of 500 μm. Survey and composition scans were conducted using a pass energy of 100 and 30 eV, respectively, using low-energy electron flooding for charge neutralization. The binding energy scales were calibrated with C 1s (284.8 eV). N_2-sorption isotherms were obtained on a Micromeritics ASAP 2420. Before measurement of the N_2-sorption isotherms, the samples were degassed at 300 °C for 6 h under vacuum. The XRD patterns of all samples were recorded on an Empyrean X-ray Diffraction System using Cu Kα radiation operating at 40 kV and 40 mA with a scan rate of 5° min^{-1}. In addition, samples reduced at 500 °C for 3 h under a stream of H_2 (60 mL min^{-1}), were characterized by XRD. The H_2-TPR experiments were carried out using a Micromeritics AutoChem II 2920 instrument to determine the reducibility of the *x*Ni–*y*Fe/Al_2O_3 catalysts. Before carrying out the measurements, the sample (0.1 g) was pretreated under flowing Ar at 300 °C for 30 min to remove any adsorbed water and other contaminants. After cooling the sample to 50 °C under a flow of Ar, it was exposed to 10% H_2/Ar mixture gas, and heated to 1000 °C at a rate of 10 °C min^{-1}. Record the hydrogen consumption during the heating process, and plot the hydrogen consumption against the temperature to obtain the H_2-TPR spectrum.

Catalytic activity tests

A catalyst sample was reduced at 500 °C in the H_2/N_2 mixture stream for 3 h before the activity test of the experiment on the amination reaction of poly(propylene glycol) monobutyl ether (PME) (25 mL) and reduced catalyst (2 g) was added to a stainless steel autoclave reactor. The reactor was sealed, replaced three times with nitrogen, and then three times with hydrogen to remove the air. Subsequently, an amount of ammonia was charged and weighed. Before the reaction, 1 MPa hydrogen was charged and heated to 220 °C for 4 h. At the end of the reaction, the water and free amine are removed from the product by spinning.

The conversion of PEA and the selectivity of primary amine were defined as follows:

$$\text{Conversion } (\%) = \frac{\text{total amine value}}{\text{hydroxyl value (OH)}}$$

$$\text{Component selectivity } (\%) = \frac{\text{primary amine value}}{\text{total amine value}}$$

Results and discussion

Fig. 1a shows the N_2 adsorption isotherms of γ-Al_2O_3 and nickel-based catalysts. According to the nomenclature of IUPAC, the isotherm of γ-Al_2O_3 exhibits iv-type isotherm and H_2-type hysteresis loops. The pore size distributions of γ-Al_2O_3 and nickel-based catalysts are shown in Fig. 1b. The pore sizes of the nickel-based catalysts are larger than that of γ-Al_2O_3.

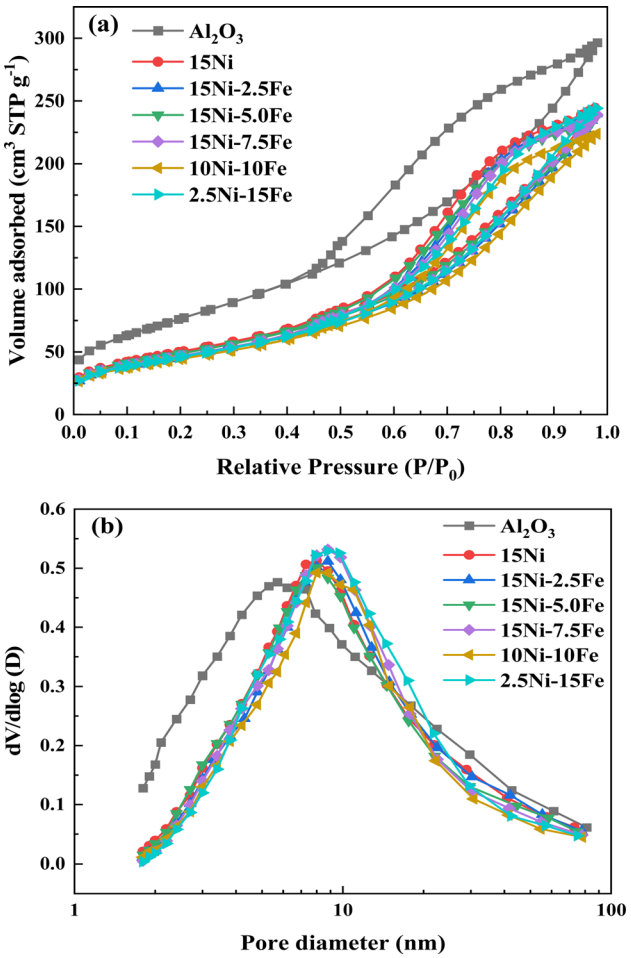

Fig. 1 (a) N_2 adsorption–desorption isotherms, and (b) pore size distributions of the *x*Ni–*y*Fe/Al_2O_3 catalysts.

The specific surface area, pore volume, and average pore size of the *x*Ni–*y*Fe/Al_2O_3 catalyst are shown in Table 1. For the support γ-Al_2O_3, the BET-specific surface area is 278.61 m^2 g^{-1}, the pore volume is 0.46 cm^3 g^{-1}, and the average pore size is 6.58 nm. After the carrier is loaded with Ni metal, the surface area of the catalyst is reduced to 181.35 m^2 g^{-1}, the pore volume of 15% Ni/Al_2O_3 decreases to 0.38 cm^3 g^{-1} and the average pore size increases to 8.34 nm. This may be because the micropores

Table 1 Textural properties of γ-Al_2O_3 and *x*Ni–*y*Fe/Al_2O_3 catalysts

Sample	S_{BET} (m^2 g^{-1})	V_{total} (cm^3 g^{-1})	D_{pore} (nm)
γ-Al_2O_3 support	278.61	0.46	6.58
15Ni	181.35	0.38	8.34
15Ni–2.5Fe	167.16	0.37	8.89
15Ni–5.0Fe	175.48	0.37	8.36
15Ni–7.5Fe	167.46	0.37	8.84
10Ni–10.0Fe	160.42	0.35	8.64
2.5Ni–15Fe	166.32	0.38	9.09

inside the carrier are clogged with the formed NiO crystals.[5] When the second metal Fe is added, the specific surface area of the catalyst is further decreased, which was 167.16 $m^2\ g^{-1}$. The catalysts with different loadings of Ni–Fe maintained average pore volumes are around 0.37 $cm^3\ g^{-1}$, and pore sizes are around 8.84 nm. After loading the bimetallic Ni–Fe, the pore structure of the catalyst does not change significantly, compared to γ-Al_2O_3.

The XRD patterns of the xNi–yFe/Al_2O_3 catalysts are displayed in Fig. 2. It can be seen that the peak ($2\theta = 44.4°$) of the 15Ni/Al_2O_3 catalyst loaded with monometallic Ni is sharper compared with that of the catalysts loaded with bimetallic Ni–Fe, indicating that the addition of the second metal Fe can improve the dispersion of the metal on the carrier.[11,12] The diffraction peaks at $2\theta = 37.6°$ and 66.7° correspond to those of γ-Al_2O_3 (JCPDS no. 29-0063). The diffraction peaks of Ni appear at $2\theta = 44.4°$ and 51.8°. The diffraction peak at $2\theta = 51.8°$ of Ni does not appear for the 2.5Ni–15Fe/Al_2O_3 catalyst due to the low Ni content. The diffraction peaks of Ni–Fe alloy have been reported to be at 44.3° and 51.5° (JCPDS no. 03-1175). For the remaining xNi–yFe/Al_2O_3 catalysts, the diffraction peaks due to Ni–Fe alloy can be found at $2\theta = 51.5°$, indicating that all four Ni–Fe loaded catalysts are formed Ni–Fe alloys. Nonetheless, 2.5Ni–15Fe/Al_2O_3 does not show alloy diffraction peaks at this position. Only the 15Ni–7.5Fe/Al_2O_3 catalyst shows a distinct diffraction peak of Ni–Fe alloy at $2\theta = 44.3°$. This indicates that the Ni–Fe alloy for 15Ni–7.5Fe/Al_2O_3 is more well-crystallized compared to the rest of the Ni–Fe bimetallic catalysts. No diffraction peaks of NiO are found in the XRD pattern, indicating that all the above catalysts are completely reduced.

The H_2-TPR curves of the xNi–yFe/Al_2O_3 catalysts after calcination at 500 °C for 3 h in air was shown by Fig. 3. The TPR curve for the 15Ni/Al_2O_3 catalyst reveals four reduction peaks at 312.5 °C, 533.1 °C, 634.7 °C, and 731.4 °C. Among them, the reduction peak at 312 °C corresponds to the reduction of NiO with larger grain size or the weak interaction of NiO-support. The reduction peaks at 552 °C and 634.7 °C, indicate the reduction of medium–strength interactions between metallic Ni and Al_2O_3 carriers, which are mainly related to the non-stoichiometric reduction of NiO and amorphous nickel aluminate spinel. The peak at 731.4 °C, is mainly caused by the reduction of $NiAl_2O_4$, which indicates a strong interaction between $NiAl_2O_4$ and Al_2O_3. By the peak area calculation in Table 2, it can be found that the catalyst consists mainly of the reduction of NiO with moderately strong interaction with the carrier.[13,14]

After the addition of the second metal Fe, by analyzing the TPR data of the Ni–Fe/Al_2O_3 catalysts, it can be found that they all show reduction peaks at 200–440 °C, 440–600 °C and 550–750 °C. By comparing with the above results, it is found that the reduction peaks at 200–440 °C represent the reduction of α-Fe_2O_3 to Fe_3O_4 and the reduction of NiO which has a weak interaction with the carrier. The reduction peaks at 400–600 °C represent the reduction of Fe_3O_4 to FeO and the reduction of NiO (which interacts strongly with the carrier) to Ni. The peaks at 600–900 °C correspond to the reduction of $NiAl_2O_4$ spinel and the reduction of iron oxide.[15,16]

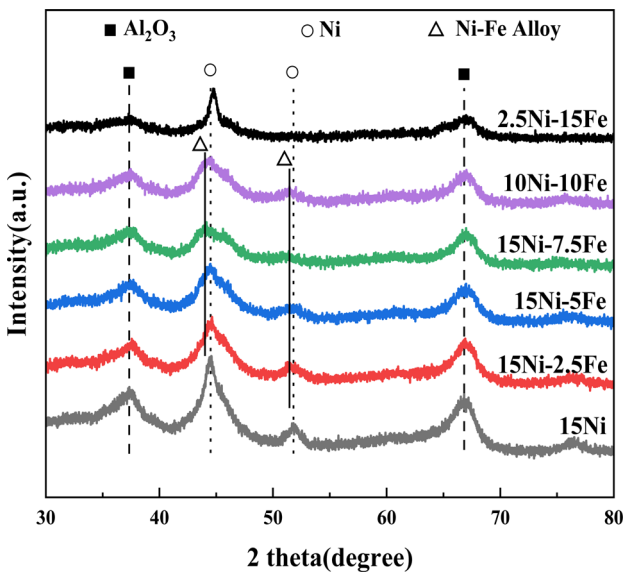

Fig. 2 XRD patterns of the xNi–yFe/Al_2O_3 catalysts.

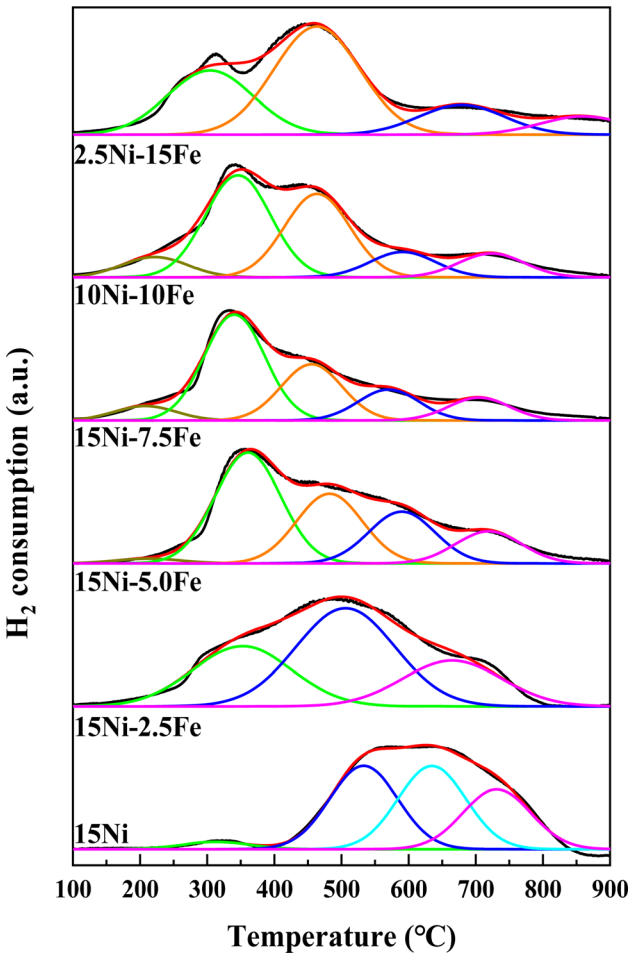

Fig. 3 H2-TPR profiles of the xNi–yFe/Al_2O_3 catalysts.

Table 2 Quantitative analysis of the percentage of reduction observed in the catalysts

	H_2-TPR peak position (°C) metal-support interaction and quantitative area (%)				
Sample	I	II	Weak	Medium	Strong
15Ni	—	—	312.5 (3.1)	533.1 (35.6), 634.7 (35.7)	731.4 (25.6)
15Ni–2.5Fe	—	—	352.4 (29.5)	506.0 (48.1)	664.9 (22.4)
15Ni–5.0Fe	212.8 (1.7)	482.12 (25.9)	360.7 (41.1)	589.9 (19.3)	719.1 (11.9)
15Ni–7.5Fe	207.8 (6.3)	455.5 (24.4)	340.5 (46.0)	570.2 (13.4)	705.0 (9.9)
10Ni–10Fe	221.74 (7.9)	463.7 (32.8)	345.8 (40.1)	591.2 (9.9)	723.4 (9.3)
2.5Ni–15Fe	—	463.35 (49.2)	304.3 (29.1)	678.98 (13.5)	859.8 (8.3)

Since unreduced NiO cannot participate in the reductive amination reaction, the position and area of the reduction peaks are closely related to the catalyst reduction performance.[5] When the Fe content is added to 5%, the reduction peak area of the catalyst gradually increases to 41.4%, and the reduction temperature increases to 360.7 °C. Interestingly, the 15Ni–7.5Fe/Al_2O_3 exhibits the largest reduction peak area (46%) and lower reduction temperature (340.5 °C) compared to other Ni–Fe catalysts. However, further addition of Fe metal results in a decrease in the area of the reduction peak. For instance, the 2.5Ni–15Fe/Al_2O_3 catalyst shows that an excessive amount of Fe metal is counterproductive. Therefore, it can be hypothesized that a moderate Ni–Fe ratio promotes the reduction of Ni–Fe bimetal-carrier interaction. Additionally, the XRD result suggests that the presence of Ni–Fe alloy makes catalysts more susceptible to reduction.

Fig. 4 shows the Ni 2p and Fe 2p XPS spectra of the *x*Ni–*y*Fe/Al_2O_3 catalysts. In Fig. 4a, the characteristic peaks of *x*Ni–*y*Fe/Al_2O_3 near 855.7 and 873.1 eV are corresponded to Ni $2p_{3/2}$ and Ni $2p_{1/2}$, respectively. For all the catalysts, the Ni^0 peaks and Ni^{2+} (NiO) peaks are detected around 852.5 eV and 855.8 eV. Compared to the other catalysts, the Ni^0 and Ni^{2+} peaks of the 15Ni–7.5Fe/Al_2O_3 catalyst shift right. This result shows that the interaction between the metal Ni–Fe and the carrier is weakened,[17] which corresponds to the H_2-TPR results mentioned above. Based on the fitted corresponding peak area ratios, the relative contents of different valence states of Ni and are calculated and the results are shown in Table 3. It can be seen that the 15Ni–7.5Fe/Al_2O_3 catalyst has the highest Ni^0 content, which is an important active substance in the reaction of dehydrogenation and hydrogenation of polyether alcohols to generate polyether amines.[18]

For the Fe 2p spectra of the *x*Ni–*y*Fe/Al_2O_3 catalysts, the main peak corresponding to Fe $2p_{3/2}$ can be observed around 710 eV. Among them, the Fe $2p_{3/2}$ spectrum can be counter-rotated into three characteristic peaks located at 707.0, 709.6, and 711.8 eV corresponding to Fe^0, Fe^{2+}, and Fe^{3+}, respectively.[5] The fitted peak areas are scaled and the results, are shown in Table 4. The result reveals that the 15Ni–7.5Fe/Al_2O_3 catalyst has the least Fe^0. This may be due to the presence of a Ni–Fe alloy, where electron transfer between Ni and Fe occurs, resulting in the conversion of Ni^{2+} to Ni^0. This interaction results in the conversion of some of the electrons from Fe^0 to Fe^{2+} or Fe^{3+}, leading to a decrease in Fe^0 content.[19] Combined with the XRD results, we can corroborate that the 15Ni–7.5Fe/Al_2O_3 catalyst possessing a distinct Ni–Fe alloy has the most catalytically active components.

Fig. 5 shows the TEM-EDS images of 15Ni–7.5Fe/Al_2O_3 catalysts. Upon analyzing the element distribution of the catalyst, it is observed that the positions of the Ni and Fe metal particles overlap. This result indicates the presence of Ni–Fe alloy on the catalyst surface. There is a slight agglomeration of these metals, likely due to the interaction between the Ni–Fe alloys.[17,20]

The conversion ratios of PME and the selectivity of primary amine (PEA) when catalyzed by 15Ni/Al_2O_3 and *x*Ni–*y*Fe/Al_2O_3 samples was shown by Fig. 6. In the catalytic amination reaction of PME, primary amines are the main products, while secondary and tertiary are the by-products.[5,6] Fig. 6 shows that adding an appropriate amount of Fe to the nickel-based catalyst enhances PME conversion, but excessive Fe has a counterproductive effect. For the selectivity of PEA, all the catalysts mentioned performed well, maintaining over 90% selectivity. Increasing the Fe content from 0 wt% (15Ni/Al_2O_3) to 2.5 wt% (15Ni–2.5Fe/Al_2O_3) enhances the conversion of PPG from 77% to 94%. Among them, the 15Ni–7.5Fe/Al_2O_3 exhibited the optimal catalytic performance with the highest conversion of PME at 99%. On the other hand, using the 2.5Ni–15Fe/Al_2O_3 in this reaction results in the conversion of PME being the lowest at 16%. This suggests that Fe metal is not the main active center and may inhibit the dehydrogenation and hydrogenation of the reactants.[5] Interestingly, while the conversion of PME increases, the selectivity of PEA shows a slightly negative correlation. In the case of the 15Ni–7.5Fe/Al_2O_3 sample, it has the highest conversion of PPG, and the selectivity of primary amine is 91%. This difference may be due to the Ni–Fe alloy increasing the number of adsorption sites and fractional coverage, leading to side effects.[10,21] Several reports have highlighted the crucial role of Ni^0 in promoting dehydrogenation and hydrogenation reactions. Supporting this, the XPS results reveal a close relationship between the conversion rate and the Ni^0 content, with 15Ni–7.5Fe/Al_2O_3 having the highest Ni^0 content and the highest conversion rate. Compared with the catalyst used in the polyether alcohol amination reaction,[6,8,22] it can be seen that the catalyst prepared in this paper has excellent performance and is not inferior to the catalyst containing precious metal components.

Fig. 7 shows the stability of 15Ni–7.5Fe/Al_2O_3 catalyst in reductive amination. We performed five cycles of experiments and the conversion rate of PPG was maintained at 99% in the

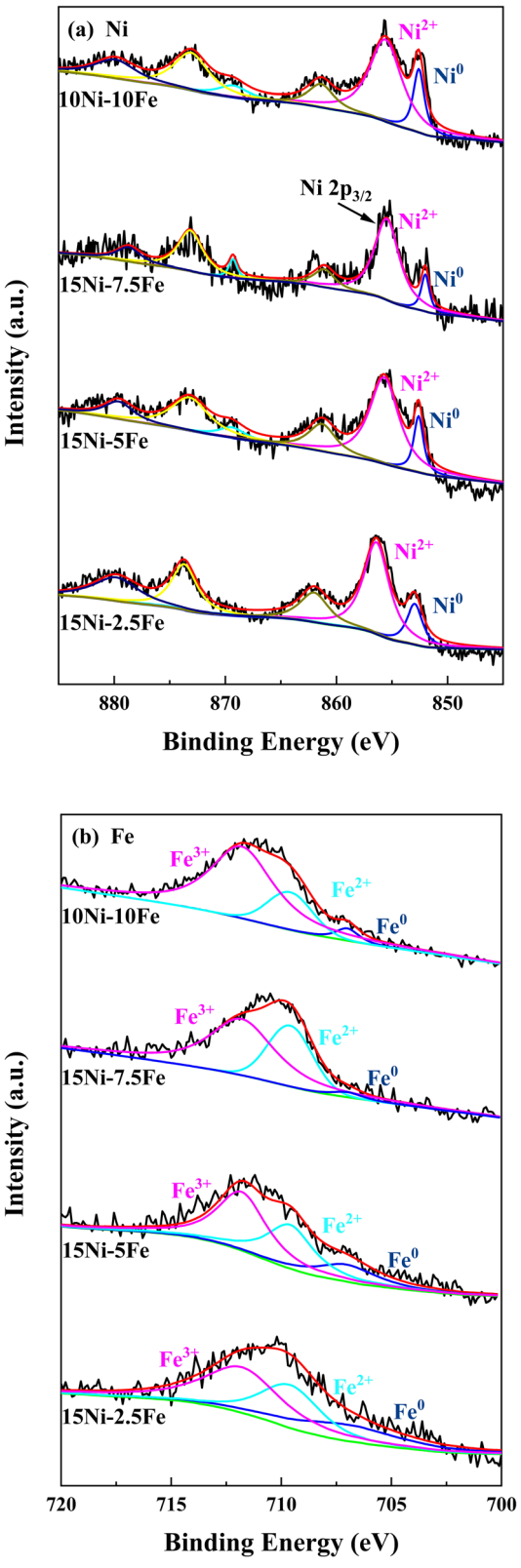

Fig. 4 XPS spectra of (a) Ni 2p, and (b) Fe 2p for the *x*Ni–*y*Fe/Al_2O_3 catalysts.

Table 3 Binding energies of Ni $2p_{3/2}$ for samples of *x*Ni–*y*Fe/Al_2O_3

Sample	Binding energy (eV) (atomic composition, %)		
	Ni^0	Ni^{2+}	Ni^0/Ni^{2+}
15Ni–2.5Fe	852.95 (21.4%)	856.4 (78.6%)	0.27
15Ni–5.0Fe	852.60 (17.9%)	855.7 (82.1%)	0.22
15Ni–7.5Fe	852.01 (24.8%)	855.46 (75.2%)	0.33
10Ni–10Fe	852.58 (21.1%)	855.58 (78.9%)	0.27

Table 4 Binding energies of Fe $2p_{3/2}$ for samples of *x*Ni–*y*Fe/Al_2O_3

Sample	Binding energy (eV) (atomic composition, %)		
	Fe^0	Fe^{2+}	Fe^{3+}
15Ni–2.5Fe	707.0 (23.4%)	709.6 (30.5%)	711.8 (46.1%)
15Ni–5.0Fe	707.0 (17.0%)	709.6 (34.3%)	711.8 (48.7%)
15Ni–7.5Fe	707.0 (2.3%)	709.6 (33.6%)	711.8 (64.1%)
10Ni–10Fe	707.0 (4.3%)	709.6 (20.0%)	711.8 (75.7%)

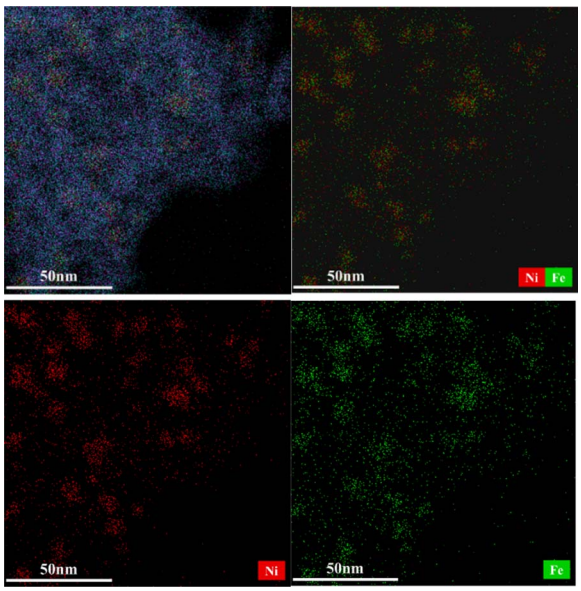

Fig. 5 TEM-EDS micrographs for the 15Ni–7.5Fe/Al_2O_3 catalysts.

first three experiments, while the conversion decreased to 82% in the fourth experiment and 60% in the fifth experiment. After five cycles of experiments, the catalyst was removed from the reactor, cleaned and centrifuged with *n*-hexane. Then the cleaned catalyst was re-put into the reaction after reduction, finding that the PPG conversion rate recovered to 99%. The results showed that the decreased activity may be caused by soluble carbon deposits blocking the catalyst pores and the catalyst structure did not collapse after five cycles. Therefore, the 15Ni–7.5Fe/Al_2O_3 catalyst showed good stability in this study and can be used in various reductive amination reaction.

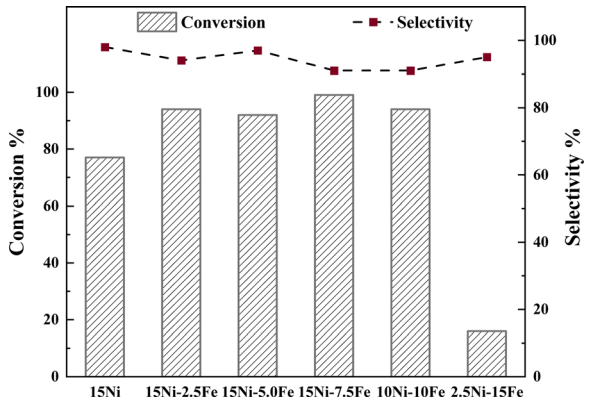

Fig. 6 The conversion ratio of PME and selectivity for the amination of PEA with NH_3 at 220 °C on the 15Ni/Al_2O_3 and xNi–yFe/Al_2O_3 reduced in H_2 at 500 °C. Other reaction conditions: t = 4 h, PME = 25 g, PME/NH_3 (mol) = 1 : 10, catalyst = 2 g.

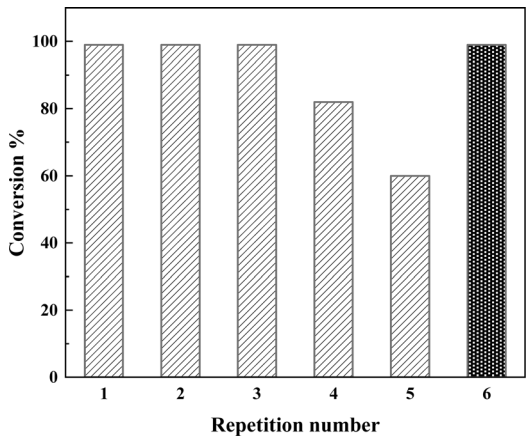

Fig. 7 The stability of the 15Ni–7.5Fe/Al_2O_3 catalyst in the reductive amination of PME. Reaction conditions: T = 220 °C, t = 4 h, PME = 50 g, PME/NH_3 (mol) = 1 : 10, catalyst = 4 g.

Conclusions

Ni–Fe bimetallic catalysts with different mass ratios loaded on γ-Al_2O_3 carrier materials were successfully prepared by isovolume impregnation method and applied in the reductive amination of polyether alcohol. From the XRD spectra and TEM-EDS results, it is known that after reduction at 500 °C for 3 h, to varying degrees, Ni–Fe alloys were formed and dispersed on the catalyst surface. The H_2-TPR results revealed that Ni–Fe alloy would affect the reduction temperature of the catalyst and contribute to an increase in the area of the Ni-related reduction peaks. In addition, the XPS results indicated that the presence of Ni–Fe alloy increased the Ni^0 content of the catalyst. The 15Ni–7.5Fe/Al_2O_3 catalyst exhibited the highest activity among all the catalysts prepared and the percent conversion of PME has not decreased after three cycles in the reductive amination. In conclusion, these results significantly demonstrated the Ni–Fe alloy can improve the activity of the catalysts, with having the highest Ni^0 content on the surface of 15Ni–7.5Fe/Al_2O_3, which led to the highest conversion rate (>99%).

Conflicts of interest

There are no conflicts to declare.

Acknowledgements

We thank the National Key R&D Program of China (No. 2021YFB3500700) for financial support.

References

1 L. J. Zhang, Y. Chao and Q. S. Yao, *Mater. Manuf. Processes*, 2014, **29**, 738.
2 M. Dryzhakov, E. Richmond and J. Moran, *Synthesis*, 2016, **48**, 935.
3 I. Aldalur, M. Armand and H. Zhang, *Batteries Supercaps*, 2020, **3**, 30.
4 A. Bayer, *US Pat.*, 4540720A, 1985.
5 E. Hong, S. Bang, J. H. Cho, K. D. Jung and C. Shin, *Appl. Catal., A*, 2017, **542**, 146.
6 H. Y. Chang, G. H. Lai, C. Y. Lin, C. Y. Lee, C. C. Chia, C. L. Hwang, H. M. Chang and D. H. Tsai, *Catal. Commun.*, 2019, **127**, 15–19.
7 C. J. Yue, L. P. Gu, Z. W. Zhang, X. J. Wei and H. S. Yang, *Arabian J. Chem.*, 2022, **15**, 103865.
8 K. Kim, Y. Choi, H. Lee and J. W. Lee, *Appl. Catal., A*, 2018, **568**, 114.
9 A. H. Braga, D. C. de Oliveira, A. R. Taschin, J. B. O. Santos, J. M. R. Gallo and J. M. C. Bueno, *ACS Catal.*, 2021, **11**, 2047.
10 J. K. Prabhakar, P. A. Apte and G. Deo, *Chem. Eng. J.*, 2023, **471**, 144252.
11 X. Xu, S. K. Megarajan, X. Xia, A. Toghan, A. Feldhoff, Y. Zhang and H. Q. Jiang, *New J. Chem.*, 2020, **44**, 18994.
12 F. H. Meng, P. Z. Zhong, Z. Li, X. X. Cui and H. Y. Zheng, *J. Chem.*, 2014, **2014**, 534842.
13 D. C. Hu, J. J. Gao, Y. Ping, L. H. Jia, P. Gunawan, Z. Y. Zhong, G. W. Xu, F. N. Gu and F. B. Su, *Ind. Eng. Chem. Res.*, 2012, **51**, 4875.
14 X. Hu, L. J. Zhang and G. X. Lu, *Appl. Catal., A*, 2012, **427**, 49.
15 R. D. P. Fiuza, M. A. D. Silva and J. S. Boaventura, *Int. J. Hydrogen Energy*, 2010, **35**, 11216.
16 S.-H. Kang, J.-H. Ryu, J.-H. Kim, S.-J. Seo, Y.-D. Yoo, P. S. Sai Prasad, H.-J. Lim and C.-D. Byun, *Korean J. Chem. Eng.*, 2011, **28**, 2282.
17 M. Cheng, J. Zhang, C. Q. Zhang, J. L. Wang, Y. Jiao, Y. Q. Chen and X. Y. Li, *Int. J. Hydrogen Energy*, 2022, **47**, 11799.
18 L. Ma, L. Yan, A.-H. Lu and Y. J. Ding, *RSC Adv.*, 2018, **8**, 8152.
19 X. Ding, T. Li, J. Q. Wang, L. Wu, L. Zheng and Y. Q. Wang, *Chem. Eng. J.*, 2023, **471**, 144668.
20 A. Tomer, B. T. Kusema, J.-F. Paul, C. Przybylski, E. Monflier, M. Pera-Titus and A. Ponchel, *J. Catal.*, 2018, **368**, 172.
21 Y. N. Wei, W. J. Ni, C. Zhang, K. Y. You, F. F. Zhao, Z. P. Chen, Q. H. Ai and H. A. Luo, *ACS Sustainable Chem. Eng.*, 2022, **10**, 13367.
22 J.-M. Jehng and C.-M. Chen, *Catal. Lett.*, 2001, **77**, 147–154.